NEUROSCIENCE

Dimensionality reduction simplifies synaptic partner matching in an olfactory circuit

Cheng Lyu[1,2]†, Zhuoran Li[1,2,3]†, Chuanyun Xu[1,2,3], Kenneth Kin Lam Wong[1,2], David J. Luginbuhl[1,2], Colleen N. McLaughlin[1,2], Qijing Xie[1,2,4]‡, Tongchao Li[1,2]§, Hongjie Li[1,2]¶, Liqun Luo[1,2]*

A navigating axon faces complex choices when selecting postsynaptic partners in a three-dimensional (3D) space. In this work, we discovered a principle that can establish the 3D glomerular map of the fly antennal lobe by reducing the higher dimensionality serially to 1D projections. During development, olfactory receptor neuron (ORN) axons first contact their partner projection neuron dendrites on the spherical surface of the antennal lobe, regardless of whether the adult glomeruli lie near the surface or inside. Along this 2D surface, axons of each ORN type take a specific, arc-shaped trajectory that precisely intersects with their partner dendrites. Altering axon trajectories compromises synaptic partner matching. A 3D search is thus reduced to one dimension, simplifying partner matching.

Proper function of the brain requires precise assembly of neural circuits during development. Serial electron microscopic reconstructions of connectivity patterns from *Caenorhabditis elegans* to mammals (*1*–*5*) have revealed unprecedented precision of neural circuit wiring. Understanding how neural circuits establish such precise synaptic connections is a central goal of neurobiology.

A fundamental open question in synaptic partner selection is how to minimize the choice for a navigating axon. Axon guidance mitigates this problem by guiding an axon to a specific brain region (*6*, *7*). At the appropriate brain region, how does an axon navigate the local three-dimensional (3D) space to find its partners among many non-partners? Some neural circuits reduce this task load by organizing target selection in lower dimensions. For example, retinotopic and layered organization in the vertebrate retina and fly optic lobe enable target selection of some visual neurons to be divided into a 1D search for a specific layer followed by a 2D search for a synaptic partner within that layer (*8*–*10*). Here, even though strictly speaking the targets still occupy a 3D physical space, we can approximate these target selection problems as 1D or 2D because the axon only needs to search in a lower-dimensional space at a given step. But for many brain structures in which synaptic partners appear to be distributed in all three dimensions, an axon would need to code for the correct movement along each of the three axes and for recognizing all potential synaptic partners within that brain region. Are there means to simplify the synaptic partner matching problem? In this work, we illustrate that in the wiring of the olfactory circuit in the fly antennal lobe, the task complexity of synaptic partner searching is effectively reduced from 3D to 1D.

[1]Department of Biology, Stanford University, Stanford, CA, USA. [2]Howard Hughes Medical Institute, Stanford University, Stanford, CA, USA. [3]Biology Graduate Program, Stanford University, Stanford, CA, USA. [4]Neurosciences Graduate Program, Stanford University, Stanford, CA, USA. ***Corresponding author. Email: lluo@stanford.edu** †These authors contributed equally to this work. ‡Present address: Calico Life Sciences LLC, South San Francisco, CA, USA. §Present address: Liangzhu Laboratory, MOE Frontier Science Center for Brain Science and Brain-machine Integration, State Key Laboratory of Brain-machine Intelligence, Zhejiang University, Hangzhou, China. ¶Present address: Huffington Center on Aging, Department of Molecular and Human Genetics, Baylor College of Medicine, Houston, TX, USA.

Projection neuron dendrites extend to the antennal lobe surface during development

In adult *Drosophila*, ~50 types of olfactory receptor neurons (ORNs) synapse with 50 types of projection neurons (PNs) in a one-to-one fashion at 50 discrete glomeruli. Each glomerulus forms a functional unit, and the 50 glomeruli together occupy stereotyped 3D positions in the antennal lobe, with some exposed to the antennal lobe surface and others exclusively interior (Fig. 1, A and B). Previous studies indicate that the assembly of the fly olfactory circuit takes sequential steps. PN dendrites first elaborate and form a coarse map (*11*, *12*). ORN axons then circumnavigate ipsi- and contralateral antennal lobes from ~18 to 32 hours after puparium formation (hours APF) (*13*, *14*). Concomitant with extending toward the contralateral antennal lobe, ORN axons send multiple transient branches in the ipsilateral antennal lobe to search for their partner PN dendrites, and those that contact dendrites of cognate PNs are stabilized (*14*, *15*) (Fig. 1A). However, the strategy that an ORN axon uses to match with partner PN dendrites remains incompletely understood. Does each ORN axon search the entire 3D space and scan through all PN types, or are there ways to reduce the number of PN candidates for each ORN type? We note that in vertebrates, glomeruli are located on the olfactory bulb surface, simplifying target selection of ORN axons to a 2D problem (*16*). Could a similar strategy be used in the developing *Drosophila* antennal lobe?

To address these questions, we began by examining the distribution of PN dendrites during development with single-type resolutions. We generated a collection of genetic drivers that label single PN types across developmental stages (Fig. 1, C to F, and fig. S1) using split-GAL4 (*17*) and Flp/FRT-based intersection strategies (*18*). Using these drivers, we compared the dendritic patterns of single PN types between the adult and the developmental stage when ORN axons start navigating the antennal lobe. We found that PNs that innervate surface and interior glomeruli in the adult antennal lobe (referred to hereafter as adult-surface and adult-interior PNs, respectively) both had parts of their dendrites at the antennal lobe surface during development (Fig. 1, C to F).

Quantitative analyses revealed that the dendritic locations of all PN types at 30 hours APF approximated their future glomerular positions in adults (Fig. 1, G and H, and fig. S1). Furthermore, dendritic distributions along the radius of the antennal lobe confirmed that all four adult-interior PN types we tested extended some of their dendrites to the antennal lobe surface, even though smaller fractions were at the surface compared with the dendritic distribution of the eight adult-surface PN types (Fig. 1I). The surface extension of adult-interior PN dendrites during development likely does not result from cognate ORN and PN interactions, as it was also observed in the same PN types at an earlier developmental stage before ORN axons had reached the antennal lobe (fig. S2). Thus, both adult-surface and adult-interior PNs extend their dendrites to the antennal lobe surface during development (Fig. 1J).

ORN axons take cell type–specific trajectories at the antennal lobe surface during development

To encounter correct partners, each ORN axon should ideally navigate along a trajectory that intersects with cognate PN dendrites. To test this hypothesis, we generated a collection of genetic drivers that label single-type or groups of ORNs across developmental stages (Fig. 2, A and B, and figs. S3 and S4). When viewed from a vertical perspective orthogonal to navigating axons, all ORN axons navigated along the spherical surface of the antennal lobe, regardless of their surface or interior positions in adults (Fig. 2B and fig. S4), in line with previous studies that examined axons in bulk (*13*, *19*).

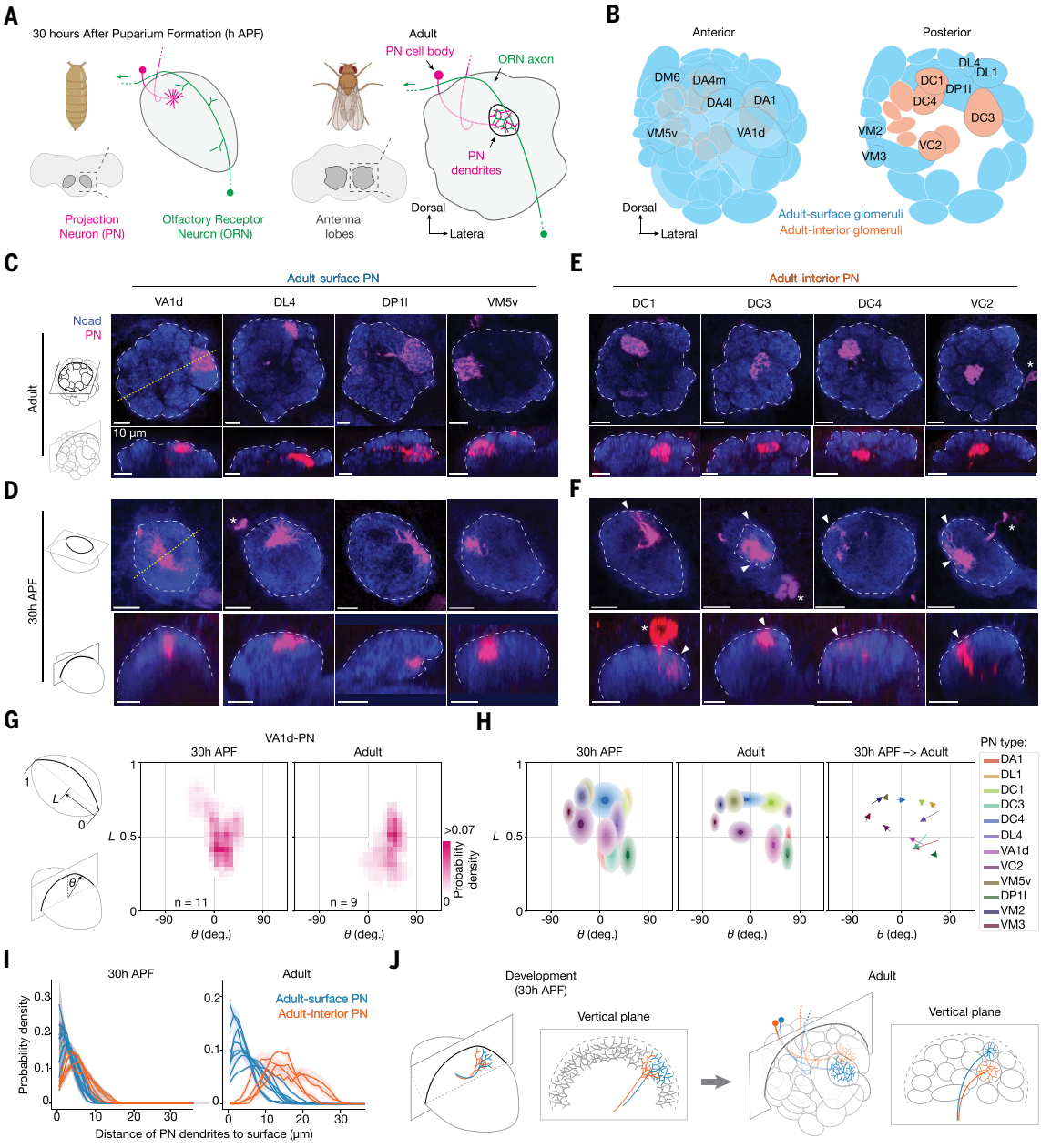

Fig. 1. During development, PN dendrites are exposed to the antennal lobe surface regardless of their position in adults. (**A**) *Drosophila* brain and antennal lobe schematics, at 30 hours APF (left) and in adults (right). Antennal lobes are highlighted in dark gray surrounded by dashed squares and are magnified to the right. At 30 hours APF, PN dendrites (magenta) innervate similar positions as in adults and ORN axons (green) navigate along the surface of the ipsilateral antennal lobe from an entry point at the bottom right toward the midline at the top left (green arrow). In adults, ORNs and PNs establish one-to-one connections in individual glomeruli that form a 3D glomerular map. (**B**) Adult antennal lobe schematic with ~50 glomeruli circled. Cyan represents glomeruli located at the surface of the antennal lobe; orange represents glomeruli located in the interior of the antennal lobe. (**C**) Optical sections showing dendrites of specific adult-surface PN types [magenta, labeled by a membrane-targeted green fluorescent protein (GFP) driven by separate genetic drivers specific to the PN types labeled above] viewed from the horizontal plane (top row) and the vertical plane (bottom row) of the antennal lobe in adults. White dashed lines outline the antennal lobe neuropil stained by the N-cadherin (Ncad) antibody (blue). Yellow dotted lines indicate the intersections with the vertical planes shown below. Vertical planes were reconstructed from 3D image volumes where optical sections were taken horizontally. The top and bottom rows show the same brains. (**D**) Same as (C), but with optical sections from 30 hours APF. (**E** and **F**) Same as (C) and (D), but for adult-interior PN types. In (F), arrowheads indicate PN dendrites extending to the antennal lobe surface; asterisks indicate PN cell bodies. In (C) to (F), scale bars are 10 µm. (**G**) Probability distribution of VA1d-PN dendritic pixels projected onto the antennal lobe surface during development (middle) and in adults (right). The 2D antennal lobe surface is flattened and decomposed into two axes: The *x* axis indicates the angle θ of each vertical plane, and the *y* axis indicates the position *L* along the long axis of the antennal lobe. A schematic definition of θ and *L* is on the left. For all genotypes, $n \geq 6$. (**H**) Probability distribution of dendritic pixels from 12 PN types projected onto the antennal lobe surface. In the left and middle panels, each ellipse corresponds to one PN type, with ellipse centers matching PN-dendrite centroids and ellipse boundaries matching the standard deviations of PN dendrites along the *x* and *y* axes, respectively. In the right panel, arrows represent how each centroid shift from 30 hours APF to adults; the color of the arrow corresponds to the ellipse in the left and middle panels. See fig. S1 for the sample number (*n*) of each group. (**I**) Probability distribution of the shortest distance in 3D space from PN dendritic pixels to the antennal lobe surface during development (left) and in adults (right). Each line represents data from an individual PN type, population mean ± SEM. (**J**) Schematics of two individual PN types during development (left) and in adults (right) viewed from +45° anterior and from a single vertical plane. Note that PN dendrites extend to the antennal lobe surface during development regardless of their surface or interior positions in adults. See table S1 for detailed genotypes.

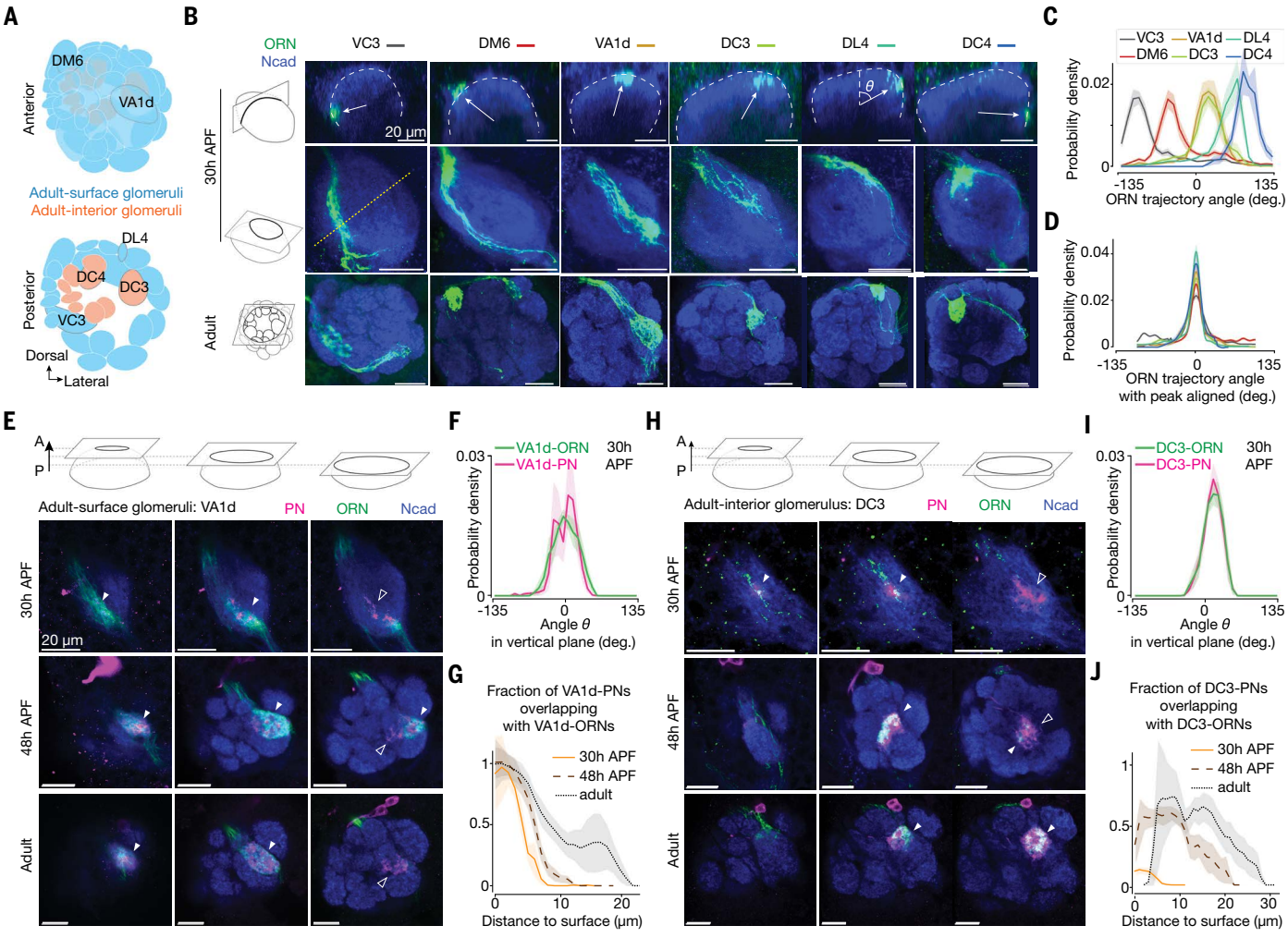

Fig. 2. During development, ORN axons take cell type–specific trajectories and contact cognate PN dendrites first on the antennal lobe surface. (**A**) Adult antennal lobe schematic highlighting six glomeruli, corresponding to the six ORN types shown in (B) to (D). (**B**) Single ORN types (green, labeled by a membrane-targeted GFP driven by separate genetic drivers) at 30 hours APF (top and middle rows, same brains) and in adults (bottom row). Shown in the top row are single optical sections from a vertical plane, with dashed lines outlining the antennal lobe neuropil stained for Ncad (blue). Vertical planes were reconstructed from 3D image volumes where optical sections were taken horizontally. Arrows point from the antennal lobe center to the average positions of ORN axons. Trajectory angle θ is defined in the DL4 panel. Shown in the middle and bottom rows are maximum projections of horizontal optical sections of antennal lobes at 30 hours APF and in adults, respectively. The yellow dotted line indicates the intersection with the vertical plane shown above. (**C**) Probability distribution of the axon's angular position from single-type ORNs at 30 hours APF. Data are population mean ± SEM. For all genotypes, $n \geq 9$. (**D**) Same as (C), but with each data curve aligned to its peak to minimize data variance between brains and more accurately reflect the width of the probability distribution. (**E**) Single optical section showing VA1d-ORNs (green, labeled by membrane-targeted GFP driven by a split-GAL4) and VA1d-PNs [magenta, labeled by membrane-targeted red fluorescent protein (RFP) driven by a split-LexA (*35*)]. Shown from left to right are anterior, middle, and posterior sections from the same brain, respectively. Filled arrowheads indicate examples where ORN axons and PN dendrites overlap; open arrowheads indicate examples where PN dendrites do not overlap with ORN axons. (**F**) Probability distribution of the angular position of VA1d-ORNs and VA1d-PNs. The definition of the angle θ is the same as in (C). Only vertical planes with PN dendrites were analyzed. Data are population mean ± SEM; $n = 9$. (**G**) Fraction of VA1d-PNs overlapping with VA1d-ORNs, as a function of the distance from PN pixels to antennal lobe surface. For a given distance on the *x* axis, a *y* value of 1 means that all the VA1d-PN dendrites within that distance bin match with VA1d-ORN axons. Data are population mean ± SEM. For all time points, $n \geq 8$. (**H** to **J**) Same as (E) to (G), respectively, but with data from DC3-ORNs and DC3-PNs. For all groups, $n = 12$. In (B), (E), and (H), scale bars are 20 μm. See table S1 for detailed genotypes.

Axons of each of the six ORN types we examined took a specific angular trajectory at 30 hours APF (Fig. 2, B to D), consistent with the positioning of their axonal tracts in adults. Some ORN types could have substantial trajectory overlaps, as observed in DC3-ORNs and VA1d-ORNs (specific ORN and PN types are named after the glomeruli they innervate, such as DC3 and VA1d). Axons from complementary ORN groups together covered the entire anterior surface of the antennal lobe (fig. S4). These findings are consistent with PN dendrites extending to specific locations at the antennal lobe surface during development and suggest that partner PN dendrites and ORN axons first meet on the 2D antennal lobe surface.

ORN axons first contact cognate PN dendrites at the antennal lobe surface

To test whether the precise locations of PN dendrites and ORN axons enable future synaptic partners to be near each other, we labeled individual ORN types and their cognate PN types with different markers in the same brain across developmental stages (Fig. 2, E and H). We observed that PN dendrites occupied a narrow angular range coinciding precisely with their cognate ORN axons (Fig. 2, F and I). For an adult-surface glomerulus, VA1d, ORNs first contacted PNs at the antennal lobe surface (Fig. 2, top row of E and orange curve in G) and maintained this into adulthood (Fig. 2, bottom rows

of E and black curves in G). For an adult-interior glomerulus, DC3, even though in adults the matching ORN axons and PN dendrites were interiorly located (Fig. 2, bottom rows of H and black curves in J), ORN axons also first contacted PN dendrites at the antennal lobe surface during development (Fig. 2, top row of H and orange curve in J).

These results suggest a working model in which individual ORN types and their cognate PNs first contact each other at the antennal lobe surface, regardless of their surface or interior positions in adults (Fig. 3A). We previously reported that two cell-surface proteins, Ten-m and Ten-a, instruct synaptic partner matching in adult-surface glomeruli through their matching expression patterns in cognate ORNs and PNs and homophilic attraction (*20*). Overexpressing Ten-m or Ten-a in adult-interior DC3-ORNs also caused mismatching phenotypes (fig. S5), suggesting that similar mechanisms are used for ORN-PN partner matching in adult-interior glomeruli. Because contact between cognate ORN and PN branches during development correlates with higher levels of filamentous actin, leading to stabilization of transient ORN axon branches (*15*), the overlaps we observed between ORN axon branches and PN dendrites at the surface could initiate synaptic partner matching. We further tested this using genetic perturbation experiments, as detailed in the next sections.

Adult-interior PNs leave more dendrites on the surface after missing cognate ORNs

If the surface-located branches from adult-interior PNs are expecting ORN partners during development, then a lack of ORN partners during development may cause these PN branches to stay at the surface, perhaps connecting with other ORN types (Fig. 3, A and B). We tested this hypothesis by genetically altering ORN trajectories in two different adult-interior glomeruli with available reagents (Fig. 3, C to K). Previous studies have shown that Sema-2b (*19*) and Toll-family proteins (*21*) are differentially expressed in ORN axons along the medial-lateral axis orthogonal to the trajectories that ORN axons take to navigate across the antennal lobe surface and also that Sema-2b instructs trajectory choice of ORN axons (*19*). Using genetic drivers that label different ORN types, we confirmed that manipulating Sema-2b and Toll expression could alter ORN trajectories during development (fig. S6). Therefore, in all the genetic perturbation experiments we performed, we rerouted specific ORN axons by combinatorially manipulating Sema-2b and Toll expression in specific ORN types.

In wild-type adults, DC4-ORN axons match DC4-PN dendrites near the center of the antennal lobe (Fig. 3D). After we experimentally rerouted most DC4-ORN axons during development, DC4-PNs no longer matched DC4-ORNs, and a portion of their dendrites remained at the

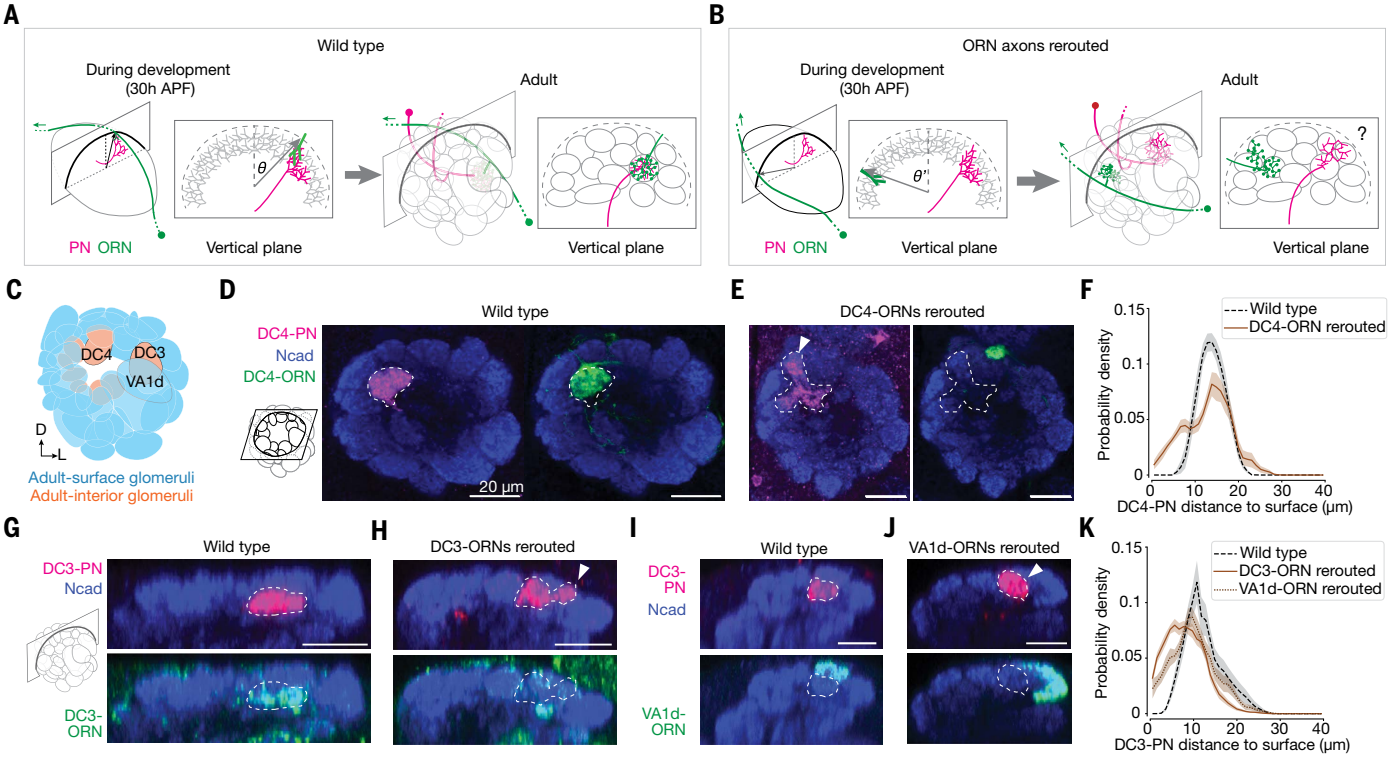

Fig. 3. Dendrites of adult-interior PNs remain at the antennal lobe surface in adults after rerouting cognate ORN axons during development. (**A**) Schematics of the same ORN-PN pair during development (left) and in adults (right). Note that DC3-ORN axons and DC3-PN dendrites are present at the antennal lobe surface during development but not in adults. (**B**) Same as (A), but with ORN axons largely rerouted and missing cognate PNs during development (left). This could lead to adult-interior PNs remaining at the surface in adults (right, indicated by a question mark). (**C**) Adult antennal lobe schematic labeling three glomeruli, corresponding to the three ORN-PN pairs shown in (D) to (J). D, dorsal; L, lateral. Some glomeruli were omitted for visualization clarity. (**D**) Single optical section of DC4-ORNs (green, labeled by membrane-targeted GFP driven by a split-GAL4) and DC4-PNs (magenta, labeled by membrane-targeted RFP driven by a split-LexA) in a wild-type brain. Dashed lines outline the boundaries of PN dendrites. (**E**) Same as (D), but with the trajectory of DC4-ORN axons changed through genetic manipulations (Toll-7 overexpression; fig. S6). The arrowhead indicates DC4-PNs innervating the antennal lobe surface. (**F**) Probability distribution of the distance from DC4-PN dendritic pixels to the antennal lobe surface in 3D space. Data are mean ± SEM. For all genotypes, $n \geq 6$. (**G** and **H**) Same as (D) and (E), but with DC3-ORNs and DC3-PNs shown in a vertical plane and a different genetic manipulation [*Toll-6* and *Toll-7* RNA interference (RNAi); fig. S6]. (**I** and **J**) Same as (G) and (H), but with the trajectory of VA1d-ORNs instead of DC3-ORNs changed through genetic manipulations (*Sema-2b* RNAi and *Toll-7* RNAi; fig. S6). (**K**) Same as (F), but with data from DC3-PNs upon the rerouting of axons from two ORN types. For all genotypes, $n \geq 11$. For (D), (E), and (G) to (J), scale bars are 20 μm. See table S1 for detailed genotypes.

antennal lobe surface in adults (Fig. 3, E and F, and fig. S7). We obtained similar findings for another adult-interior glomerulus, DC3 (Fig. 3, G, H, and K). With DC3-ORNs rerouted, some surface dendrites of DC3-PNs appeared postsynaptic to ORN axons innervating the surface VA1d glomerulus exterior to the DC3 glomerulus (fig. S8). Given that these rerouting experiments involved specific and small perturbations to the olfactory system, the inward movement of adult-interior PN dendrites is not likely to be caused passively by global antennal lobe morphogenesis but rather requires interactions of PN dendrites with their cognate ORN axons.

To examine the nature of the force that drives this inward movement, we genetically rerouted axons of VA1d-ORNs, which target the VA1d glomerulus external to the DC3 glomerulus (Fig. 3, C and I, and fig. S7). This rerouting also caused DC3-PN dendrites to remain at the antennal lobe surface in adults (Fig. 3, J and K, and fig. S7). This nonautonomous effect from manipulating neighboring glomeruli suggests that axons and dendrites of adult-interior ORNs and PNs are pushed inward by neurites from nearby adult-surface glomeruli.

The accuracy of ORN-PN matching correlates with the accuracy of ORN trajectories

Our results thus far suggest a model in which the dimensionality of partner selection for each ORN type can be further reduced from two dimensions to one dimension: Each ORN type only searches for synaptic partners within a 1D narrow stripe near its axon trajectory (fig. S9). To further test this model, we examined how the accuracy of the ORN axon trajectory affects the accuracy of ORN-PN partner matching. If each ORN type only searches within the vicinity of its trajectory, then changing its trajectory should impair ORN-PN partner matching, with the degree of trajectory deviation determining the degree of mismatching. Using genetic drivers that label specific ORN types across developmental stages, we performed genetic manipulations in specific ORN types and altered their trajectories to different degrees in both directions during development. We then labeled cognate ORNs and PNs with distinct markers in the same adult brain and calculated the fraction of ORN axons that overlaps with dendrites of cognate PNs as a measure for the accuracy of ORN-PN partner matching (Fig. 4).

Taking the VA1d-ORNs as an example (Fig. 4, A to D), we used three genetic manipulation strategies that combinatorially manipulated the expression of Sema-2b and the Toll proteins in VA1d-ORNs to alter the ORN trajectories during development to three different distributions deviating from the wild-type distribution (Fig. 4, top row of A, and B and C). In adults, we observed different degrees of mismatching between the VA1d-ORNs and VA1d-PNs (Fig. 4, bottom rows of A, and D). We repeated this type of experiment in three other ORN types and observed similar results (Fig. 4, E to P).

Manipulating the expression of Sema-2b and the Toll proteins may affect not only ORN axon trajectories but also other processes that might influence ORN-PN partner matching. The following evidence suggests that the ORN-PN mismatching we observed is largely due to the change of ORN trajectories. In all cases, the portion of ORNs that mismatched with cognate PNs in adults were likely the portion of ORNs whose axons deviated from the wild-type position during development. For example, a comparison of "Manipulation #1" with "Wild type" (first two columns of Fig. 4A) shows that the VA1d-ORN trajectory partly deviated counterclockwise during development (top row of Fig. 4A); in adults, the VA1d-ORNs that mismatched with VA1d-PNs also moved counterclockwise (appearing to move leftward in the lower rows). The fact that data from all the manipulation conditions followed this trend strongly suggests that synaptic partner matching is most likely due to trajectory changes rather than other effects caused by the change in Sema-2b or Toll protein expression (which presumably happens in all manipulated ORN axons, whether the trajectory is changed or not).

Furthermore, when grouping all the data, we observed a strong positive correlation between the accuracy of ORN axon trajectories during development and the accuracy of ORN-PN matching in adults (Fig. 4Q), indicating that the further ORN axons deviate from their normal positions, the more severe the ORN-PN mismatch that occurs. These data support the model that each ORN axon searches for synaptic partners within a narrow stripe near its axon trajectory on the antennal lobe surface, approximating a 1D space (fig. S9).

Discussion

In this work, we discovered that the repeated use of the dimensionality reduction principle simplifies the synaptic partner matching problem in the assembly of the fly olfactory circuit: For each ORN type, instead of selecting 1 out of 50 PN types in a 3D volume, the ORN only needs to select one out of a few PN types along a 1D trajectory (fig. S9). A linchpin of this work has been the collection of genetic drivers that label many individual PN and ORN types across development. Although single–cell type labeling in the adult fruit fly is becoming routine (*22*, *23*), genetic drivers that consistently label specific cell types across development are more difficult to generate because of the dynamic nature of gene expression throughout development. Our work shows that such drivers, once generated, allow systematic examination of the same neurons at high resolution across development. This led to the discovery of PN dendrite surface extension and the coincidence of partner PN dendrites and ORN axons at the surface, two key bases for our model. These drivers also allowed us to simultaneously manipulate the expression of multiple genes in specific cell populations across development to test the model. Our dataset included glomeruli innervated by ORNs from both antenna and maxillary palp, which reach the antennal lobe at different times (*24*); it also included glomeruli innervated by PNs that contribute to only the adult antennal lobe and to both larval and adult antennal lobes (*25*). Thus, dimensionality reduction likely applies generally to the fly olfactory system. A systematic approach of generating cell type–specific drivers throughout development (*26*) can propel mechanistic understandings of more developmental processes.

In principle, searching for synaptic partners in a lower-dimensional space reduces simultaneous choices at any given time and thus could increase wiring accuracy and robustness. Indeed, some circuits are apparently organized following the dimensionality reduction principle, as exemplified by the distribution of glomeruli on the surface of the vertebrate olfactory bulb. In other circuits where synaptic targets are seemingly distributed in 3D space, as in the fly antennal lobe, the dimensionality reduction principle may nevertheless apply. For example, in the fly optic lobe and vertebrate retina, target selection across different layers often occurs within a 1D columnar structure (*8*, *9*), which, in some cases, is followed by a 2D search of synaptic partners within a specific layer (*10*). Further, axons of a specific retinal ganglion cell type connect with their target in the correct retinotopic position and a specific sublayer in the superior colliculus (*27*, *28*). During development, retinal ganglion cell axons could divide the 3D search task to a 2D retinotopic mapping with a 1D search for a specific sublayer. Lastly, axons of callosal projecting neurons in the mammalian cortex not only target appropriate cortical areas in the contralateral hemisphere but also terminate at specific layers (*29*, *30*). During development, these axons first navigate via the corpus callosum to appropriate cortical areas before ascending to specific layers (*29*, *31*), converting a 3D target-selection problem into sequential 2D and 1D problems. Thus, dimensionality reduction might be a widely used strategy for selecting synaptic partners in developing nervous systems.

What molecular mechanisms might be involved in executing the dimensionality reduction strategy? As is evident from the fly olfactory circuit, a coordinated patterning of pre- and postsynaptic partners is required. First, PNs must target dendrites to type-specific 2D

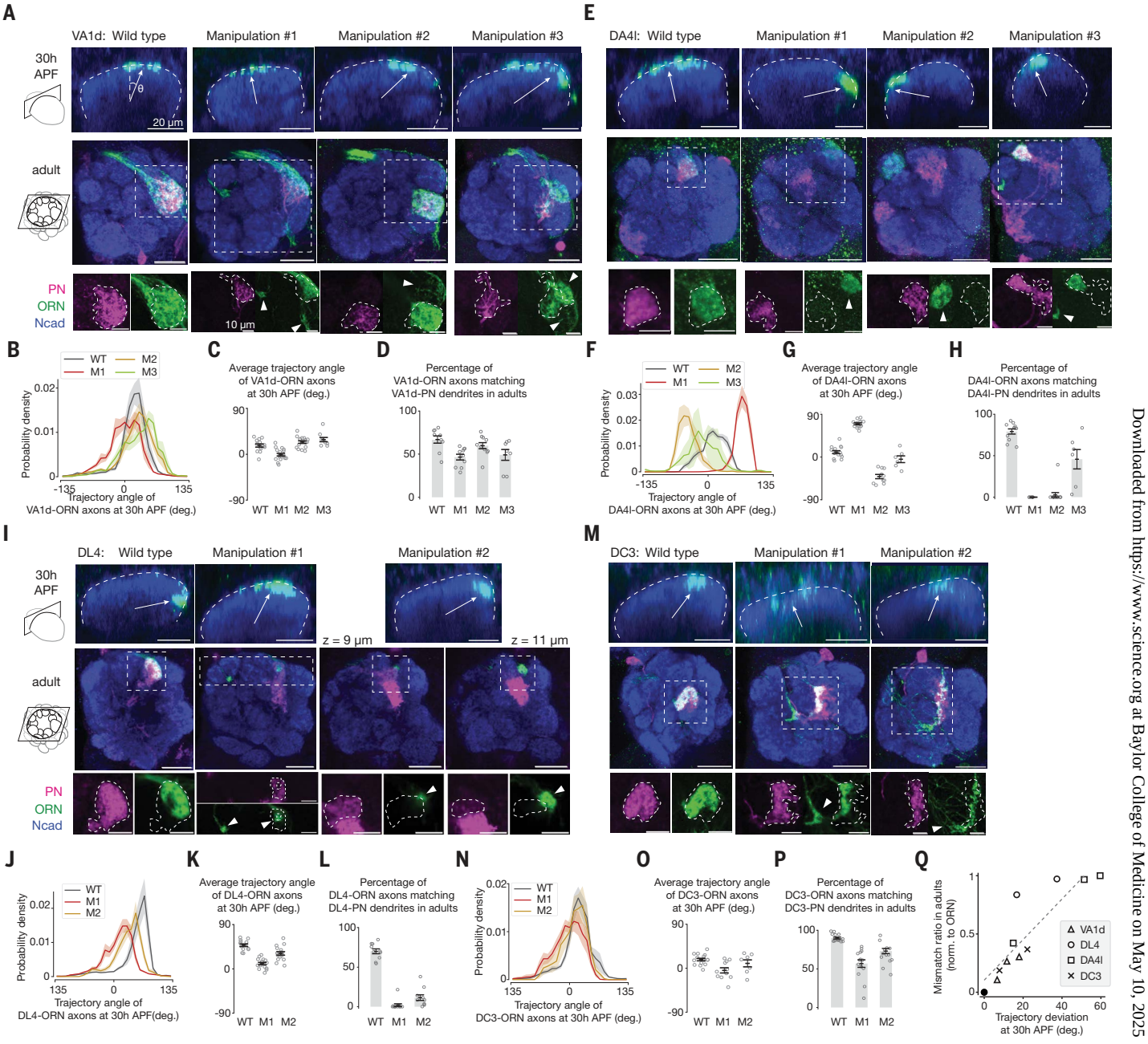

Fig. 4. The accuracy of ORN-PN synaptic partner matching correlates with the accuracy of ORN trajectories. (**A**) Single optical sections showing VA1d-ORN axons from a vertical view during development (top) and horizontal view in adult (middle and bottom). In the top row, dashed lines outline the antennal lobe neuropil. Arrows point from the antennal lobe center to the average positions of ORN axons. Images in the bottom row are magnified views of the regions enclosed by the dashed squares in the middle row. In the bottom row, dashed lines outline the boundary of PN dendrites. Arrowheads indicate ORN axons mismatching with cognate PN dendrites. The three manipulation conditions are (1) *Sema-2b* RNAi, (2) *Toll-7* RNAi, and (3) *Sema-2b* RNAi and *Toll-7* RNAi. (**B**) Probability distribution of the angular position of VA1d-ORN axons in each condition at 30 hours APF. Data are population mean ± SEM. For all genotypes, $n \geq 6$. WT, wild type; M, manipulation condition. (**C**) Average angular position of VA1d-ORN axons in each condition. Data are the same as in (B). Circles indicate the averages of individual antennal lobes; bars indicate the population mean ± SEM. (**D**) Percentage of VA1d-ORN axons overlapping with VA1d-PN dendrites in adults. Circles indicate the average of individual antennal lobes; bars indicate the population mean ± SEM. (**E** to **H**) Same as (A) to (D), respectively, but for DA4l-ORNs and DA4l-PNs. The three manipulation conditions are (1) *Sema-2b* RNAi; (2) *Toll-6* RNAi, *Toll-7* RNAi, and Sema-2b overexpression; and (3) *Toll-6* RNAi and *Toll-7* RNAi. Note that owing to reagent limitations, the ORN signals from the top row result from a combination of three ORN types: DA4l, DA4m, and DC1, all of which take a similar trajectory (fig. S3). (**I** to **L**) Same as (A) to (D), respectively, but for DL4-ORNs and DL4-PNs. The two manipulation conditions are (1) Sema-2b overexpression and (2) *Toll-6* RNAi, *Toll-7* RNAi, and Sema-2b overexpression. (**M** to **P**) Same as (A) to (D), respectively, but for DC3-ORNs and DC3-PNs. The two manipulation conditions are (1) *Toll-7* RNAi and (2) *Toll-7* RNAi and *Sema-2b* RNAi. (**Q**) Percentage of ORN-PN mismatch in adults as a function of the absolute angular changes in ORN axon trajectory at 30 hours APF, with each manipulation condition represented by a data point. Only the population means are shown. The black dot indicates wild type in each ORN type, which is the origin ($x = 0, y = 0$) in the plot by definition. The dashed line indicates the linear fit. The Pearson correlation coefficient is equal to 0.88; $p = 3.6 \times 10^{-4}$. Note that DL4 deviates most from the linear fit; this is likely to be because the DL4 glomerulus is in the middle of the DL4-ORN axon trajectory and is thus more sensitive to trajectory angle changes (than glomeruli located near the ORN axon entry point before axons with different trajectories fully diverge). In (A), (E), (I), and (M), scale bars are 20 μm in the first and second rows and 10 μm in the third row. See table S1 for detailed genotypes.

areas of the antennal lobe surface. Semaphorins and leucine-rich-repeat cell-surface proteins have been shown to instruct global targeting and local segregation of PN dendrites, respectively (*32*–*34*). We do not know what mechanisms ensure that all PN types extend at least part of their dendrites to the antennal lobe surface or what causes PN dendrites and ORN axons that target interior glomeruli to descend after they first contact each other at the surface. Our rerouting experiments suggest that the latter process likely involves competition with neurites from neighboring glomeruli. Second, ORN axons must choose type-specific trajectories according to their types. Sema-2b plays an instructive role (*19*) and we further implicated Toll receptors in this study, but more molecules are likely required to fully specify ORN axon trajectories. Third, along the chosen 1D trajectory, ORN axons must select dendrites from one out of several PN types to form synaptic connections. Homophilic attraction molecules such as teneurins play a role in this process (*15*, *20*), but more molecules are likely involved. We note that the dimensionality reduction strategy also enables combinatorial use of wiring molecules; for example, synaptic partner–matching molecules can be combined with different trajectory-selection molecules so that they can be reused along spatially segregated 1D trajectories. Finally, all of the wiring molecules we have discussed are evolutionarily conserved from invertebrates to mammals, raising the possibility that they also contribute to executing the dimensionality reduction strategy in the wiring of the more complex mammalian brain.

REFERENCES AND NOTES

1. J. G. White, E. Southgate, J. N. Thomson, S. Brenner, *Philos. Trans. R. Soc. London Ser. B* **314**, 1–340 (1986).
2. K. L. Briggman, M. Helmstaedter, W. Denk, *Nature* **471**, 183–188 (2011).
3. S. Loomba *et al.*, *Science* **377**, eabo0924 (2022).
4. P. Schlegel *et al.*, *Nature* **634**, 139–152 (2024).
5. S. Dorkenwald *et al.*, *Nature* **634**, 124–138 (2024).
6. B. J. Dickson, *Science* **298**, 1959–1964 (2002).
7. A. L. Kolodkin, M. Tessier-Lavigne, *Cold Spring Harb. Perspect. Biol.* **3**, a001727–a001727 (2011).
8. J. R. Sanes, S. L. Zipursky, *Neuron* **66**, 15–36 (2010).
9. J. R. Sanes, S. L. Zipursky, *Cell* **181**, 536–556 (2020).
10. E. Agi *et al.*, *Science* **383**, 1084–1092 (2024).
11. G. S. X. E. Jefferis *et al.*, *Development* **131**, 117–130 (2004).
12. K. K. L. Wong *et al.*, *eLife* **12**, e85521 (2023).
13. M. Okumura, T. Kato, M. Miura, T. Chihara, *Genes Cells* **21**, 53–64 (2016).
14. T. Li *et al.*, *Cell* **184**, 5107–5121.e14 (2021).
15. C. Xu *et al.*, *Cell* **187**, 5081–5101.e19 (2024).
16. K. Mori, H. Sakano, *Annu. Rev. Neurosci.* **34**, 467–499 (2011).
17. H. Luan, N. C. Peabody, C. R. Vinson, B. H. White, *Neuron* **52**, 425–436 (2006).
18. K. G. Golic, S. Lindquist, *Cell* **59**, 499–509 (1989).
19. W. J. Joo, L. B. Sweeney, L. Liang, L. Luo, *Neuron* **78**, 673–686 (2013).
20. W. Hong, T. J. Mosca, L. Luo, *Nature* **484**, 201–207 (2012).
21. A. Ward, W. Hong, V. Favaloro, L. Luo, *Neuron* **85**, 1013–1028 (2015).
22. L. Tirian, B. J. Dickson, bioRxiv 198648 [Preprint] (2017); https://doi.org/10.1101/198648.
23. G. W. Meissner *et al.*, *eLife* **12**, e80660 (2023).
24. L. B. Sweeney *et al.*, *Neuron* **53**, 185–200 (2007).
25. E. C. Marin, R. J. Watts, N. K. Tanaka, K. Ito, L. Luo, *Development* **132**, 725–737 (2005).
26. Y. D. Chen *et al.*, *Proc. Natl. Acad. Sci. U.S.A.* **120**, e2307451120 (2023).
27. D. A. Feldheim, D. D. M. O'Leary, *Cold Spring Harb. Perspect. Biol.* **2**, a001768–a001768 (2010).
28. I.-J. Kim, Y. Zhang, M. Meister, J. R. Sanes, *J. Neurosci.* **30**, 1452–1462 (2010).
29. S. P. Wise, E. G. Jones, *J. Comp. Neurol.* **168**, 313–343 (1976).
30. S. Pal, J. W. C. Lim, L. J. Richards, *Curr. Opin. Neurobiol.* **84**, 102837 (2024).
31. J. Zhou *et al.*, *Proc. Natl. Acad. Sci. U.S.A.* **110**, E2714–E2723 (2013).
32. T. Komiyama, L. B. Sweeney, O. Schuldiner, K. C. Garcia, L. Luo, *Cell* **128**, 399–410 (2007).
33. W. Hong *et al.*, *Nat. Neurosci.* **12**, 1542–1550 (2009).
34. L. B. Sweeney *et al.*, *Neuron* **72**, 734–747 (2011).
35. C. Y. Ting *et al.*, *Genetics* **188**, 229–233 (2011).

ACKNOWLEDGMENTS

We thank the labs of G. Rubin, N. Perrimon, Y. Aso, T. Lee, and T. Chihara; the Bloomington *Drosophila* Stock Center, the Vienna *Drosophila* Resource Center, and the Kyoto *Drosophila* Stock Center for fly stocks; H. Dionne and G. Rubin for many enhancer plasmids; K. Shen and H. Deng for their generous help with super-resolution microscopy; and S. Block and J. Luo, as well as members of the Luo laboratory, especially D. Paderick and T. Hindmarsh Sten, for helpful discussions. **Funding:** This work was supported by National Institutes of Health grant R01-DC005982 (to L.L.). C.L. was supported by the Stanford Science Fellows Program. L.L. is a Howard Hughes Medical Institute investigator. **Author contributions:** C.L., Z.L., and L.L. conceived the project. C.L. and Z.L. performed all of the experiments and analyzed the data. C.L., Z.L., and L.L. jointly interpreted the data and decided on new experiments. C.X. and K.K.L.W. assisted in cloning and immunostaining. D.J.L., K.K.L.W., C.N.M., Q.X., T.L., and H.L. assisted in the generation of transgenic flies. C.L., Z.L., and L.L. wrote the paper, with input from all other co-authors. L.L. supervised the work. **Competing interests:** The authors declare that they have no competing interests. **Data and materials availability:** All data are included in the manuscript or the supplementary materials.

SUPPLEMENTARY MATERIALS

science.org/doi/10.1126/science.ads7633
Materials and Methods; Figs. S1 to S9; Table S1; References (*36*–*43*); MDAR Reproducibility Checklist

Submitted 27 August 2024; resubmitted 30 December 2024; accepted 20 February 2025

10.1126/science.ads7633